Acta Crystallographica Section A
Foundations of Crystallography
ISSN 0108-7673

Received 12 February 2004
Accepted 3 June 2004

On functions and quantities derived from the experimental electron density

Vladimir Tsirelson[a,b]* and Adam Stash[c]

[a]Mendeleev University of Chemical Technology, Miusskaya Square 9, 125047 Moscow, Russia, [b]Institute of Physics, University of Augsburg, Augsburg 86135, Germany, and [c]Karpov Institute of Physical Chemistry, ul. Vorontsovo pole 10, 103064 Moscow, Russia. Correspondence e-mail: tsirel@muctr.edu.ru

Calculation of properties of molecules and crystals as obtained from a multipole electron-density model restored from the accurate X-ray diffraction data is considered. Electronic and exchange energy-density distributions are presented along with those of local temperature and local entropy. Integration of the local functions over atomic basins defined by the zero-flux condition allows properties of molecules and crystals to be expressed in terms of atomic contributions derived directly from X-ray diffraction experiments. Distributions of local Fermi momentum and one-electron potential are considered as well. The approach has been applied to diamond, sodium fluoride, sodium chloride, solid chlorine, α-oxalic acid dihydrate and $YBa_2Cu_3O_{6.98}$.

1. Introduction

A description of bonding in molecules and solids in terms of the electron density (ED) and electron-density-based functions is a quickly developing field, which is known to attract physicists, chemists, biologists, geochemists and materials scientists. Analysis of total, valence and deformation electron densities and electrostatic potential, the gradient and Laplacian fields has developed into an effective tool for quantitative evaluation of physical and chemical properties of molecules and solids[1] (Bader, 1990; Tsirelson & Ozerov, 1996). The main language of such works is that of the topological theory of atomic and molecular interactions developed by Bader (1990) and others. On the other hand, ED, which determines all properties of atoms, molecules and crystals in the ground electronic state (Hohenberg & Kohn, 1964), is a main variable in the density functional theory (DFT). This well established theory (Springborg, 1977; Lundqvist & March, 1983; Dahl & Avery, 1984; Parr & Yang, 1989; Dreizler & Gross, 1990; Reznik, 1992; Ellis, 1995; Nagy, 1998; Kohn, 1999) provides a basis for a quantitative determination of electronic properties in terms of local kinetic, potential and total electronic energies, density of exchange energy and exchange potential. Since ED has become readily obtainable from the accurate X-ray, γ-ray and synchrotron-radiation diffraction experimental data *via* the multipole expansion model (Tsirelson & Ozerov, 1996), a combination of the DFT formalism and model electron density may be used to analyze the nature of atomic and molecular interactions in solids. The model quasistatic ED is as precise as ~0.05 e Å^{-3} in the main part of a crystal space; the regions around the nuclei with radius of about 0.2 Å, where experimental error increases with the atomic number, are excluded. The model ED is close to that derived from quantum mechanics (Tsirelson, 2002*a*,*b*,*c*); therefore, it appears to be suitable for the analysis of bonding mechanisms.

In practice, the exact functionals connecting physical functions and quantities with the electron density are often unknown. This is true *e.g.* for kinetic energy as well as for exchange and correlation energy functionals. As a result, DFT methods use approximate functionals with explicit dependence on ED (Parr & Yang, 1989; Dreizler & Gross, 1990; Reznik, 1992). Unlike the orbital scheme of Kohn & Sham (1965), such an approach makes the variational determination of wavefunctions completely unnecessary, in accordance with the Hohenberg & Kohn (1964) formulation of the DFT. For example, the kinetic energy density can be approximated according to Kirzhnits (1957) *via* electron density and its derivatives (Tsirelson, 1992). Espinosa *et al.* (1998, 1999) and Espinosa & Molins (2000) have extended this approach to the potential energy density using a local virial theorem (Bader, 1990). Later, Espinosa *et al.* (2001), Galvez *et al.* (2001) and Tsirelson (2002*a*,*b*,*c*, 2003) strengthened this approach by demonstrating that the approximate quasistatic model ED yields the kinetic, potential and total electronic energy distributions in close agreement with those obtained from first principles. Tsirelson (2002*a*) has also discussed the specificity of using the model electron density derived from an X-ray diffraction experiment in the DFT formalism and pointed out the limitations of this approach. Tsirelson & Stash (2002*a*,*b*) approached a quantum-chemical description even more closely by extending it to the approximate determination of the electron localization function and localized-orbital locator.

[1] Electric dipole and quadrupole molecular moments (Spackman, 1992), the electrostatic part of the intermolecular energy (Suponitsky *et al.*, 1999) and the electric field gradient at the position of a nucleus (Tsirelson & Ozerov, 1996) are also known to provide information on bonding.

The Dirac–Slater exchange potential calculated using experimental ED was presented as well (Stash & Tsirelson, 2002).

Experimental ED-based determination of local energy and related properties has been widely used to analyze bonding in molecules and solids, mainly by evaluation of the topological parameters at the bond critical points (Cramer & Kraka, 1984; Bader, 1990; Bone & Bader, 1996; Abramov, 1997; Hill *et al.*, 1997; Martin Pendas *et al.*, 1977, 1998; Luana *et al.*, 1997; Espinosa *et al.*, 1998, 1999; Tsirelson *et al.*, 1998; Spackman, 1999; Bianchi *et al.*, 2000; Gibbs *et al.*, 2000; Popelier *et al.*, 2000; Zhurova & Tsirelson, 2002; Tafipolsky *et al.*, 2002; Scherer *et al.*, 2003). At the same time, Popelier (2000) and Tsirelson (2003) found that the critical-point-based description of bonding is rather incomplete, whereas analysis of the ED and energy distribution over the entire molecular or crystal space provides a more detailed picture of the bonding.

In this work, we further explore possible use of the experimentally derived electron density and its derivatives in the approximate functionals of the density functional theory. We present distributions of the total electronic energy density and exchange energy density and consider the atomic contributions of these functions in average energy properties of many-electron systems. We also extend the latter approach to the 'internal' thermodynamic properties of the electron gas such as local temperature and local entropy. And finally, we show that a local Fermi momentum and a one-electron potential (Hunter, 1975, 1986, 1996) derived from the experimental electron density can serve as a descriptor of electron localization. Physical and chemical content of these functions will be illustrated by a number of examples of compounds with different types of chemical bonds.

We should mention that all the functions considered in this work, in principle, might also be calculated using the one-electron density matrix reconstructed from the electron density with different methods (Tsirelson *et al.*, 1977; Tsirelson & Ozerov, 1979; Clinton *et al.*, 1983; Gritsenko & Zhidomirov, 1987; Levy & Goldstein, 1987; Aleksandrov *et al.*, 1989; Schwarz & Mueller, 1990; Schmider *et al.*, 1992; Zhao & Parr, 1993; Jayatilaka, 1998; Jayatilaka & Grimwood, 2004). Tsirelson & Ozerov (1996) have discussed the advantages and pitfalls of the last approach in detail.

2. An overview

The local electronic energy characterizing the bonding in many-electron systems (Bader & Beddall, 1972),

$$h_e(\mathbf{r}) = g(\mathbf{r}) + v(\mathbf{r}), \tag{1}$$

is a sum of the density of the quasiclassical electronic kinetic energy

$$g(\mathbf{r}) = (1/2)\nabla_{\mathbf{r}}\nabla_{\mathbf{r}'}\gamma(\mathbf{r},\mathbf{r}')|_{\mathbf{r}=\mathbf{r}'} \tag{2}$$

[$g(\mathbf{r}) \geq 0$] and the negative-everywhere density of the electronic potential energy

$$v(\mathbf{r}) = -\sum_a [Z_a/(\mathbf{r}-\mathbf{R}_a)]\rho(\mathbf{r}) + \int [\Gamma(\mathbf{r},\mathbf{r}_1)/(\mathbf{r}-\mathbf{r}_1)]\,\mathrm{d}\mathbf{r}_1 + V_{\mathrm{en}} \tag{3}$$

(atomic units are used throughout the paper). Here, $\gamma(\mathbf{r},\mathbf{r}')$ and $\Gamma(\mathbf{r},\mathbf{r}_1)$ are one- and two-electron density matrices, Z_a is the charge of a nucleus a placed at $\mathbf{R}_a$ and V_{en} stands for the electron–nuclear attraction term. The sign of $h_e(\mathbf{r})$ shows that either kinetic or potential energy dominates at a given point $\mathbf{r}$.

DFT considers electron density in molecules and solids to be an inhomogeneous gas of non-interacting electrons. Realization of the Hohenberg–Kohn approach implies that the local homogeneity principle (Kirzhnits *et al.*, 1975) is imposed, *i.e.* the property density at each point $\mathbf{r}$ is supposed to be the same as that of a homogeneous electron gas with ED equal to $\rho(\mathbf{r})$ everywhere. The latter approximation, which is widely used in the DFT, makes the results obtained for a homogeneous electron gas applicable in the case of inhomogeneous systems. Accordingly, the Thomas–Fermi model of an electron gas (Parr & Yang, 1989) is often used in the description of the electronic structure of molecules and crystals as an initial approximation.

The one-electron density matrix $\gamma(\mathbf{r},\mathbf{r}')$ in (2) is related to the one-particle Green function *via* the Laplace transformation (Parr & Yang, 1989; Dreizler & Gross, 1990). Using the gradient $\hbar$ expansion of the Green function around the classical Thomas–Fermi term (Kirzhnits, 1957), the kinetic energy density may be expressed *via* electron density and its derivatives:

$$g_{\mathrm{DFT}}(\mathbf{r}) = (3/10)(3\pi^2)^{2/3}\rho(\mathbf{r})^{5/3} + (1/72)[\nabla\rho(\mathbf{r})]^2/\rho(\mathbf{r}) + (1/6)\nabla^2\rho(\mathbf{r}). \tag{4}$$

The first term in (4) is the Thomas–Fermi kinetic energy density. Though the latter expansion is not unique owing to the Laplacian term (Cohen, 1979, 1984; Cohen & Zaparovanny, 1980), it satisfies a necessary non-negativity condition for the phase-space function representing the quasiprobability distribution of electrons over coordinates and momenta (Ayers *et al.*, 2002). The long-range behavior of the approximate $g_{\mathrm{DFT}}(\mathbf{r})$ is correct provided that the gradient expansion is truncated at the second-order term (Tal & Bader, 1978). At the same time, the approximate function $g_{\mathrm{DFT}}(\mathbf{r})$ [equation (4)] attains unphysical negative values with $r \rightarrow R_i$ because of the Laplacian term, whereas the 'correct' kinetic energy density $g(\mathbf{r})$ [equation (2)] is finite and positive at the nuclei (Bader & Beddall, 1972). Fortunately, the radius of negative holes in $g(\mathbf{r})$ surrounding the nuclei does not exceed 0.15 Å, attaining the maximum for an H atom, which is within the range of error resulting from the experimental uncertainty of ED in the vicinity of the nuclei.

The local form of the virial theorem (Bader & Beddall, 1972)

$$2g(\mathbf{r}) + v(\mathbf{r}) = (1/4)\nabla^2\rho(\mathbf{r}) \tag{5}$$

relates $g(\mathbf{r})$ and $v(\mathbf{r})$ with the Laplacian of ED. Thus, having estimated $g(\mathbf{r})$ from expression (4), we can determine the potential energy density $v(\mathbf{r})$ using (5) and then calculate the

density of the total electronic energy (1), provided that $\rho(\mathbf{r})$, $\nabla\rho(\mathbf{r})$ and $\nabla^2\rho(\mathbf{r})$ are known. The experimental electron density may be used to carry out these calculations (Tsirelson, 1992, 2002*a*; Espinosa *et al.*, 2001; Espinosa & Molins, 2000).

Approximation (4) allows us to extend the list of functions, derivable from the experimental ED. According to Ghosh *et al.* (1984), the position distribution of electrons at any point is described by the local Maxwell–Boltzmann distribution law. The local kinetic energy and the local temperature characterize this electron motion, and there is no current density in a stable system due to electron movement in all directions. The local internal temperature of an electron gas can be written as (Ghosh *et al.*, 1984)

$$t(\mathbf{r}) \cong (2/3k_{\rm B})g_{\rm DFT}(\mathbf{r})/\rho(\mathbf{r}), \qquad (6)$$

where $k_{\rm B}$ is the Boltzmann constant. The associated entropy density is

$$s(\mathbf{r}) \cong (3/2)k_{\rm B}\rho(\mathbf{r})\{\lambda + \ln[g_{\rm DFT}(\mathbf{r})/g_{\rm TF}(\mathbf{r})]\}, \qquad (7)$$

where $g_{\rm TF}(\mathbf{r})$ is the Thomas–Fermi kinetic energy density and

$$\lambda = 5/3 + \ln(4\pi c_{\rm TF}/3), \quad c_{\rm TF} = (3/10)(3\pi^2)^{2/3}.$$

The local temperature is different from the external temperature and the local entropy is different from the true entropy: thermodynamic properties are zero for the electronic ground state, whereas local functions $t(\mathbf{r}) \geq 0$ and $s(\mathbf{r}) \geq 0$ are $\mathbf{r}$-dependent. The temperature (6) locally measures the kinetic electronic energy per particle at an external temperature equal to 0 K. The local entropy (7) measures (up to a constant) the deviation of the electron distribution from that of the Thomas–Fermi model at point $\mathbf{r}$ (Nagy & Parr, 2000).

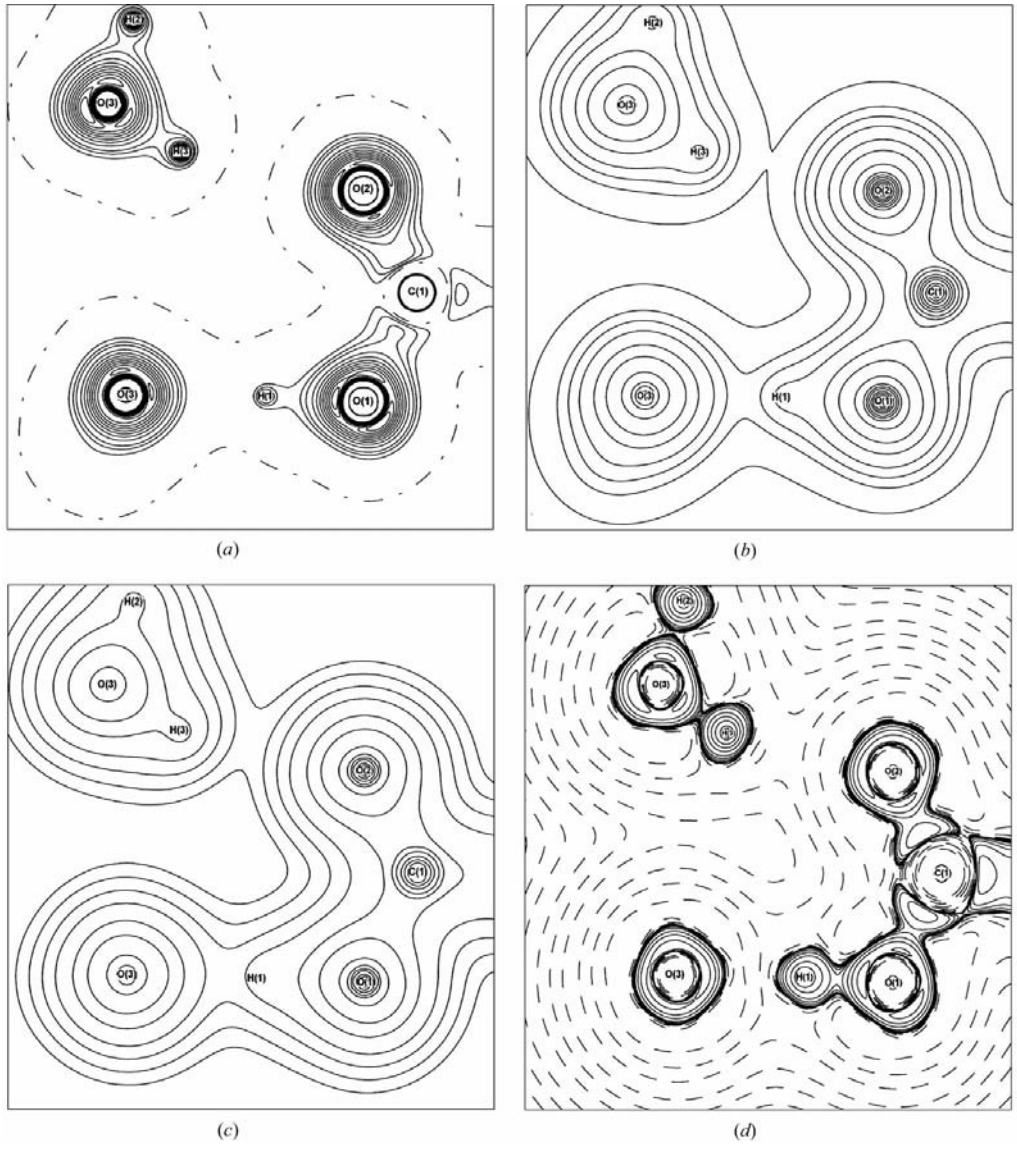

Figure 1
Distributions of (*a*) the total electronic energy and (*b*) exchange energy as well as (*c*) the electron density and (*d*) Laplacian of the electron density in crystalline α-oxalic acid dihydrate, $C_2H_2O_4{\cdot}H_2O$. Line intervals are $\pm(2, 4, 8)\nabla \times \nabla 10n$ atomic units ($-2 \leq n \leq 2$). In (*a*), (*b*) and (*d*) negative values are solid; zero contours are dot-dashed; in (*c*) positive values are solid.

Some other functions widely used in solid-state and molecular physics and quantum chemistry may be also expressed *via* ρ(r), $\nabla\rho$(r) and $\nabla^2\rho$(r). First, we mention the gradient-corrected exchange energy density, ε_x, which may be expressed for the closed-shell systems as (Becke, 1988)

$$\varepsilon_x = -\alpha\rho^{4/3}(\mathbf{r}) - (1/2)^{1/3}\frac{bX^2}{1+6bX\sinh^{-1}(X)}\rho(\mathbf{r})^{4/3}. \quad (8)$$

Here

$$\alpha = \tfrac{3}{4}\left(\frac{3}{\pi}\right)^{1/3}, \quad b = 0.0042, \quad X = 2^{1/3}\frac{|\nabla\rho(\mathbf{r})|}{\rho(\mathbf{r})^{4/3}} \quad (9)$$

[spin density $\rho_\sigma(\mathbf{r})$ was assigned the value of $(1/2)\rho$(r)]. This function explicitly reveals regions of the potential-energy lowering caused by exchange between electrons of the same spin.

Another example is the one-electron potential (Hunter, 1975, 1986)

$$P(r) = \nabla^2\rho(\mathbf{r})/4\rho(\mathbf{r}) - |\nabla\rho(\mathbf{r})|^2/8[\rho(\mathbf{r})]^2, \quad (10)$$

which is an exact solution of a one-electron Schrödinger equation. The one-electron potential determines the potential energy of (any) one electron in a many-electron system and enters the effective potential in Kohn–Sham equations (Levy *et al.*, 1984). According to Hunter, the negative areas of $P(\mathbf{r})$ correspond to positive values of local one-electron kinetic energy, meaning that an electron is classically allowed in these areas. On the contrary, positive values of $P(\mathbf{r})$ reveal potential barriers where electrons exhibit quantum behavior. The second term in (10) is always negative, whereas the first term has the same sign as $\nabla^2\rho(\mathbf{r})$. Thus, classically allowed regions of $P(\mathbf{r})$ correspond to regions of negative Laplacian of the electron density – an empirical indicator of electron concentration in Bader's (1990) theory of atomic interactions. It is essential that the one-electron potential of any free atom exhibits alternating negative minima and positive maxima revealing the shell structure while the Laplacian of the electron density does not exhibit such behavior for outer electron shells of some atoms beginning with the fourth row of the Periodic Table (Sagar *et al.*, 1988; Shi & Boyd, 1988; Kohout *et al.*, 1991; Kohout, 2001). The latter circumstance has an important practical consequence. Lack of regions with $\nabla^2\rho(\mathbf{r}) < 0$ prevents the application of a standard topological approach to study the chemical bond in compounds containing heavy atoms. In this case, the one-electron potential can serve as a useful descriptor of details of the atomic interactions.

Finally, we mention the local Fermi momentum

$$k_{\rm F}(\mathbf{r}) = (3\pi^2)^{1/3}\rho^{1/3}(\mathbf{r}), \quad (11)$$

which characterizes the electron velocity associated with the Fermi energy in the Thomas–Fermi homogeneous electron–gas model. We can hardly treat $k_{\rm F}$ as a measure of the electron velocity in real crystals. However, as a consequence of the local homogeneity principle (Kirzhnits *et al.*, 1975), $k_{\rm F}$ depends on **r** and is a convenient tool to recover tiny bonding details in the regions with near-uniform low (~0.1–0.3 e Å^{-3}) electron density.

3. Results and discussion

We shall apply the approach outlined above to compounds whose electron density was described by the Hansen & Coppens (1978) multipole model. Multipole parameters used in calculations were taken from the following sources: Abramov & Okamura (1997) for diamond, Scherer (2004) for α-oxalic acid dihydrate, Stash *et al.* (2004) for NaF and NaCl and Stevens (1979) for Cl_2. Multipole parameters for $YBa_2Cu_3O_{6.98}$ were obtained by Stash (2003) using experimental structure factors from Lippmann *et al.* (2003). All the results described in this work were obtained using program *WinXPRO2003* (Stash & Tsirelson, 2002). Wavefunctions by Macchi & Coppens (2001) were used in the calculations.

3.1. Distributions of the electronic and exchange energies

A typical picture of the total electronic energy distribution (1) is given in Fig. 1(*a*), where $h_e(\mathbf{r})$ is plotted for crystalline α-oxalic acid dihydrate, $C_2H_2O_4\cdot H_2O$. In the solid state, six water molecules surround each molecule of acid and the intermolecular hydrogen bonds exist along with intramolecular covalent interactions. The energy density attains its lowest negative values on the intra- and intermolecular bond lines, revealing areas of concentration associated with bonding interactions and lone pairs.[2] Simultaneously, alternating negative minima and positive maxima observed in the vicinity of nuclei exhibit the shell structure of bonded O and C atoms.

The map of $h_e(\mathbf{r})$ allows one to distinguish a shorter O(1)—H(1)···O(3) hydrogen bond from a longer one, O(3)—H(3)···O(2). Indeed, both hydrogen bonds are characterized by different depth local minima $h_{e,\rm min}$ of −0.0340 and +0.0055 a.u., respectively. A similar behavior of $h_e(\mathbf{r})$ in crystalline urea has been reported elsewhere (Tsirelson, 2002*a*).

A map of the local exchange energy, ε_x, drawn in the same plane (Fig. 1*b*) shows the contribution of the electron exchange to the total electronic energy. Besides deep energy wells in the vicinity of the nuclei, it also reveals the negative exchange-energy-density bridges between bonded atoms contributing to the potential-energy lowering during crystal formation. Magnitudes of exchange contributions depend on the nature of the bond, *e.g.* the shorter hydrogen bond in $C_2H_2O_4\cdot H_2O$ is characterized by a lower value of $\varepsilon_x < 0$ than its longer counterpart (Fig. 1*b*). Function $-\varepsilon_x$ looks like the electron density shown in Fig. 1(*c*): it implicitly contains all typical bonding features such as valence-electron concentrations and lone pairs, which become evident with the help of the Laplacian of the electron density (Fig. 1*d*). However, there is no need to analyze the Laplacian of $-\varepsilon_x$: the Laplacian electron density itself provides us with this information.

[2] These features cannot be attributed to the presence of the Laplacian term in the Kirzhnits approximation (4): the Hartree–Fock electronic energy density exhibits the same features.

The closer the DFT local exchange energy approaches its quantum-mechanical counterpart, the more accurate are the electronic properties that result from a DFT calculation. We believe that the analysis of the exchange-energy density derived from experimental electron density in different approximations may be used to improve existing DFT functionals and therefore can open the way to a more accurate prediction of electronic properties of matter.

3.2. Local temperature and local entropy

In the vicinity of the nuclei ($r \rightarrow R_i$), the local temperature $t(\mathbf{r})$ approaches $Z_i^2/(3k_B)$, Z_i is the nuclear charge. In isolated atoms, $t(\mathbf{r})$ exhibits a decreasing stepwise variation with $\mathbf{r}$ showing characteristic values for the different atomic shells (Nagy *et al.*, 1996). In molecules and solids, the sphericity of the distribution of $t(\mathbf{r})$, typical in the free atom, is destroyed by bonding interactions. Indeed, the local temperature of the H_2O molecule (in α-oxalic acid dihydrate) decreases along the O—H bonds and in the vicinity of electronic lone pairs of the O atom (Fig. 2*a*). The difference map of the local temperature referred to the promolecule, a superposition of undistorted atoms calculated using wavefunctions by Macchi & Coppens (2001), reveal this feature even better (Fig. 2*b*). Recalling that $t(\mathbf{r})$ is a local measure of the kinetic electronic energy per particle, we conclude that charge accumulations in molecular position space cause the electron velocity and, consequently, the local temperature to decrease. Thus, the local temperature reveals the accumulations of electronic charge commonly associated with bonds and lone pairs.

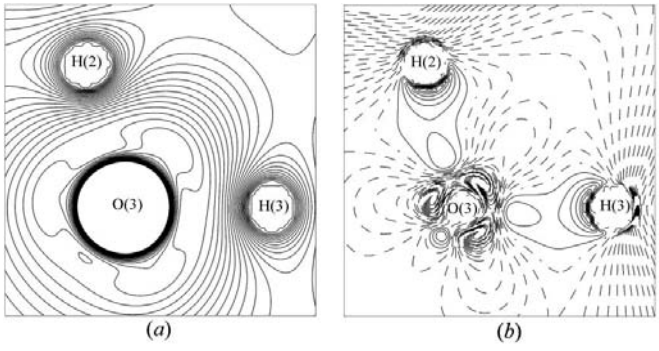

Figure 2
(*a*) Distribution of the local temperature in the water molecule (removed from crystalline α-oxalic acid dihydrate, $C_2H_2O_4{\cdot}H_2O$) and (*b*) corresponding difference map of the local temperature relative to the promolecule. Line intervals are: (*a*) 0.05 k_BT and (*b*) 0.02 k_BT. Areas of relative temperature decrease in (*b*) are shown by solid lines.

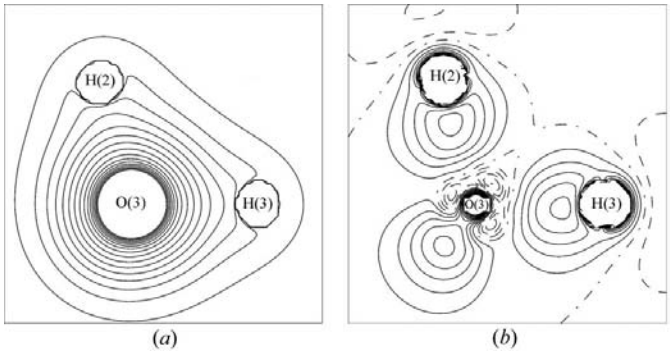

Figure 3
(*a*) Distribution of the local entropy in the water molecule (removed from a crystalline α-oxalic acid dihydrate, $C_2H_2O_4{\cdot}H_2O$) and (*b*) corresponding difference map of the local entropy relative to the promolecule. Line intervals are: (*a*) 0.5 s/k_B and (*b*) 0.05 s/k_B. Areas of relative temperature decrease in (*a*) and areas of relative entropy increase in (*b*) are shown by solid lines.

Local entropy of the electron density, $s(\mathbf{r})$, attains a maximum at $r \rightarrow R_i$ and decreases monotonically with increasing r. It resembles the electron-density distribution shown in Fig. 3(*a*) and does not explicitly exhibit any bonding features. At the same time, the 'difference' map of $s(\mathbf{r})$ referred to the promolecule reveals the latter features very well (Fig. 3*b*).

Since an approximate model for the kinetic energy density is known to fail for H atoms (Tsirelson, 2002*a*; Tsirelson & Stash, 2002*a*), we carried out the 'difference' local electron temperature and entropy calculations for diamond (Fig. 4). Again, the electron accumulations in the covalent bond cause the local temperature to increase and the local entropy to decrease compared to the promolecule. Thus, conclusions drawn for the water molecule remain valid in spite of the deficiency in the H-atom description.

We note that 'difference' maps for $t(\mathbf{r})$ and $s(\mathbf{r})$ exhibit the double-humped profiles, typical for the valence-electron density of a C—C bond in diamond, whereas the corresponding deformation ED shows a single bonding peak.

Simultaneously, profiles of the Laplacian of $t(\mathbf{r})$ and $s(\mathbf{r})$ clearly reveal the C—C bonding features (Fig. 5). Indeed, the temperature field (*i.e.* the kinetic electronic energy per particle) of the electron gas is concentrated between the C atoms with a slight depletion in the middle of the bond, whereas near constant entropy reveals a local electron concentration in that area.

3.3. Atomic contributions to electronic and exchange energies

According to Bader (1990), the position space of a molecule or crystal may be divided into atomic basins separated by surfaces satisfying the zero-flux condition

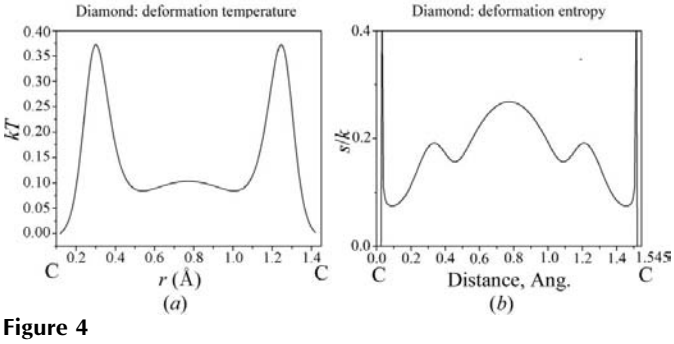

Figure 4
(*a*) The difference local electron temperature $\delta t(\mathbf{r}) = t_{\mathrm{procryst}}(\mathbf{r}) - t_{\mathrm{cryst}}(\mathbf{r})$ and (*b*) difference entropy $\delta s(\mathbf{r}) = s_{\mathrm{procryst}}(\mathbf{r}) - s_{\mathrm{cryst}}(\mathbf{r})$ along the C—C bond in diamond.

$$\nabla\rho(\mathbf{r})\cdot n(\mathbf{r}) = 0, \quad \forall \mathbf{r} \in S_i(\mathbf{r}). \tag{12}$$

These basins are identified with bonded atoms (pseudoatoms), an integral of any property, $A(\mathbf{r})$, over the volume of such an atom, Ω,

$$\langle A\rangle = \int_{\Omega} \mathbf{A}(\mathbf{r})\,\mathrm{d}V, \tag{13}$$

yielding an average value of the property, whereas the sum of atomic contributions thus obtained yields the value of the property for a whole system. If this is applied to $h_e(\mathbf{r})$ and ε_x, Bader's approach may be used to obtain energies of functional atomic groups, bonded molecules or elementary cells in a crystal. Atomic components of electronic energy for H_2O (in α-oxalic acid dihydrate), NH_3 and Cl_2 molecules removed from the crystal are given in Table 1. After summing, they yield the electronic energy of a molecule. Note that integrated energy values of h_e do not depend on the Laplacian term in expression (4): the integral of $\nabla^2\rho(\mathbf{r})$ over the atomic basins was 0.0 ± 10^{-3} a.u.; the latter number is an error due to integration. Quantum-chemically calculated values obtained for free molecules (Table 1) indicate that our approach provides a reasonable agreement between experimental and theoretical energies, in spite of the slight distortions induced in experimental electron densities from the parent crystal environment. The largest discrepancy of 1.7% obtained for the Cl_2 molecule may be attributed to a relatively low accuracy of the corresponding X-ray diffraction experiment. We note, however, that, even in the case of perfect X-ray diffraction data, energies of intermolecular interaction or cohesion cannot be obtained in this way since their typical values are comparable with experimental uncertainty.

The atomic integrated values of the exchange energy, $E_{\rm exch}$, temperature, T, and entropy, S, as well as corresponding molecular values are also given in Table 1. Maximal $E_{\rm exch}$ discrepancy of 2.5% is again observed for the Cl_2 molecule, although overall agreement between experimentally derived and Hartree–Fock exchange energies is good. Listed values of temperature and entropy in Table 1 may be considered as predictions. Now we can only say that integrated T and S values for N and O atoms are close to those given in the literature for free atoms (Chattaraj *et al.*, 1999).

Table 1
Atomic contributions to the electronic energy, h_e, exchange energy, $E_{\rm exch}$, local temperature, T, and local entropy, S, calculated from the model electron densities.

The total molecular values are also listed and compared with the Hartree–Fock values given in parentheses. All values are given in atomic units.

Atom or molecule	h_e	$E_{\rm exch}$	kT	S/k
H_2O				
O	−75.743	−8.759	32.219	59.036
H	−0.298	−0.162	2.868	2.907
H	−0.296	−0.160	2.880	2.870
Total	−76.337 (−76.171†)	−9.081 (−8.946‡))	37.967	64.813
NH_3				
N	−55.300	−7.129	33.604	54.366
H	−0.301	−0.171	3.572	3.242
Total	−56.204 (−56.326†)	−7.642 (−7.670‡)	44.320	64.092
Cl_2				
Cl	−451.517	−26.887	47.857	108.215
Total	−903.034 (−918.892)	−53.774 (−55.094‡)	95.714	216.430

† Iyengar *et al.* (2001). ‡ Lee & Zhou (1991).

3.4. One-electron potential

A map of the one-electron potential $P(\mathbf{r})$ in the Cl_2 molecule calculated from the experimental electron density using (10) is shown in Fig. 6(*a*). A comparison with a theoretical calculation of Chan & Hamilton (1998) (Fig. 6*b*) demonstrates that the experimental $P(\mathbf{r})$ reveals both electron concentrations associated with lone pairs and charge depletion at the centre of the Cl—Cl bond reported earlier (Tsirelson *et al.*, 1995). Our calculations of the one-electron potentials for α-oxalic acid dihydrate, urea and S_4N_4 confirm that $P(\mathbf{r})$ visualizes charge concentrations and depletions in agreement

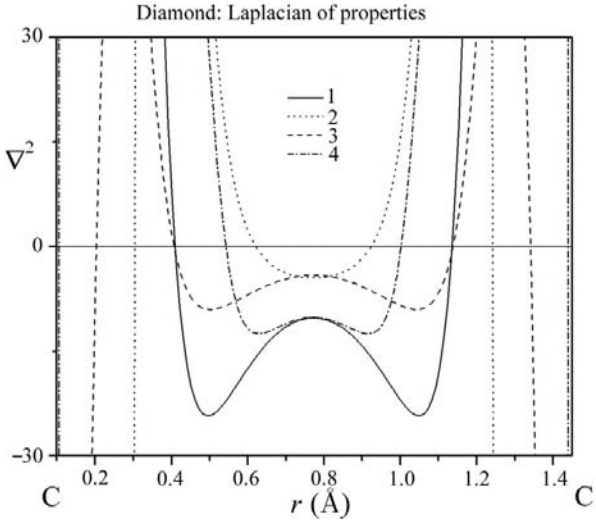

Figure 5
Distributions of the Laplacians of electron density (1), local temperature (2), local Fermi momentum (3) and local entropy (4) along the C—C bond in diamond.

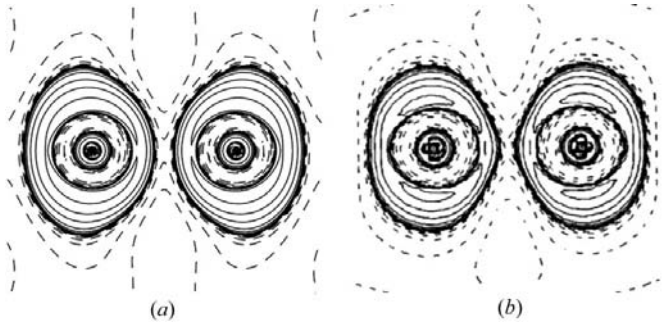

Figure 6
Distributions of the one-electron potential in the Cl_2 molecule (*a*) calculated using the model electron density derived from the X-ray diffraction experiment and (*b*) calculated by Chan & Hamilton (1998) using DFT. Line intervals are $\pm(2, 4, 8) \times 10^n$ atomic units, solid lines correspond to the negative values of the one-electron potential indicated by the charge concentrations.

Table 2
Topological parameters of the bond critical points in the electron density and in the Fermi momentum for the anion–anion interactions in NaCl and NaF.

	NaCl	NaF
$\rho_{\text{b.c.p.}}$	0.030 (5)	0.027 (6)
λ_1	−0.10 (3)	−0.12 (2)
λ_2	−0.05 (2)	−0.01 (2)
λ_3	0.47 (2)	0.59 (2)
$\nabla^2\rho_{\text{b.c.p.}}$	0.32 (2)	0.46 (2)
$k_{F\ \text{b.c.p.}}$	0.51	0.491
$\lambda_1(k_F)$	−0.57	−0.72
$\lambda_2 k_F)$	−0.27	−0.07
$\lambda_3(k_F)$	2.68	3.56
$\nabla^2 k_{F\ \text{b.c.p.}}$	1.84	2.77

with conclusions drawn by Chan & Hamilton (1998, 1999) and Levit & Safarti (1997) on the basis of DFT calculations.

We tested the ability of the one-electron potential to analyze chemical bonding in a heavy-atom compound, $YBa_2Cu_3O_{6.98}$. Since the features of the of Ba—O interaction in $YBa_2Cu_3O_{6.98}$ cannot be resolved with the help of $\nabla^2\rho$, let us consider the Ba—O(4) bonding interaction in the O—Ba—O plane of this crystal. Integration of the electron density over zero-flux atomic basins yields atomic charges of +1.48 (2) and −0.86 (2) e for Ba and O, respectively. This is in accordance with the general point of view that the Ba–O interaction is of the closed-shell type; however, the details of this interaction are not evident.

Kohout *et al.* (1991) pointed out that the Laplacian of ED does not resolve the outermost *P* electronic shell of the Ba atom. Moreover, this is true even for the penultimate *O* shell of Ba because the corresponding extrema of $\nabla^2\rho(\mathbf{r})$ are positive. In contrast, the atomic one-electron potential of Ba exhibits areas with $P(\mathbf{r}) < 0$ corresponding to both *O* and *P* shells. In a crystal, outermost electron concentrations of Ba and O fall into a region of the interference of valence orbitals of the two atoms (Fig. 7*a*), where electrons are classically allowed. Here $P(\mathbf{r}) < 0$ reveals an accumulation of electrons resulting from the charge transfer from Ba to O. The Ba—O bond critical point in the electron density is 1.511 Å from the Ba atom: it falls within the area of $P(\mathbf{r}) > 0$, corresponding mainly to the outer region of the O shell of the Ba atom, which is a manifestation of the ionic character of the bonded Ba atom.

3.5. Fermi momentum

The local Fermi momentum can also be used to analyze the details of an electron density distribution. Because the pattern of the (3, −1) critical points in the Fermi momentum distribution coincides with that of the electron density, the Fermi momentum gradient field may help to identify bond critical points in areas characterized by near-uniform low (0.1–0.3 e Å^{-3}) values of $\rho(\mathbf{r})$. For example, Tsirelson *et al.* (1998) found that, in the case of the electron density reconstructed with the κ model, the principal ED curvature λ_2 approaches zero at the critical points on the F—F and Cl—Cl interaction lines in NaF and NaCl, respectively. Shallow ED surfaces prevent the recognition with confidence of the type of critical bond on the anion–anion line. At the same time, topological parameters of the local Fermi momentum, which are more sensitive to **r** dependence, allows one to identify the latter as bond critical points (Table 2).

We have also found that the Laplacian of k_F reveals electron concentrations and depletions in the same way as the Laplacians of the electron density, local electron temperature and entropy (Fig. 5). The same conclusion may be drawn from the analysis of the $\nabla^2 k_F$ distribution along the Ba—O bond in $YBa_2Cu_3O_{6.98}$ (Fig. 7*b*), which is in agreement with the consideration given above for the one-electron potential. Thus, $\nabla^2 k_F$ could also be used as another localization function.

In conclusion, a combination of the diffraction technique with functionals of the density functional theory leads to the unification of the theoretical and experimental methods and

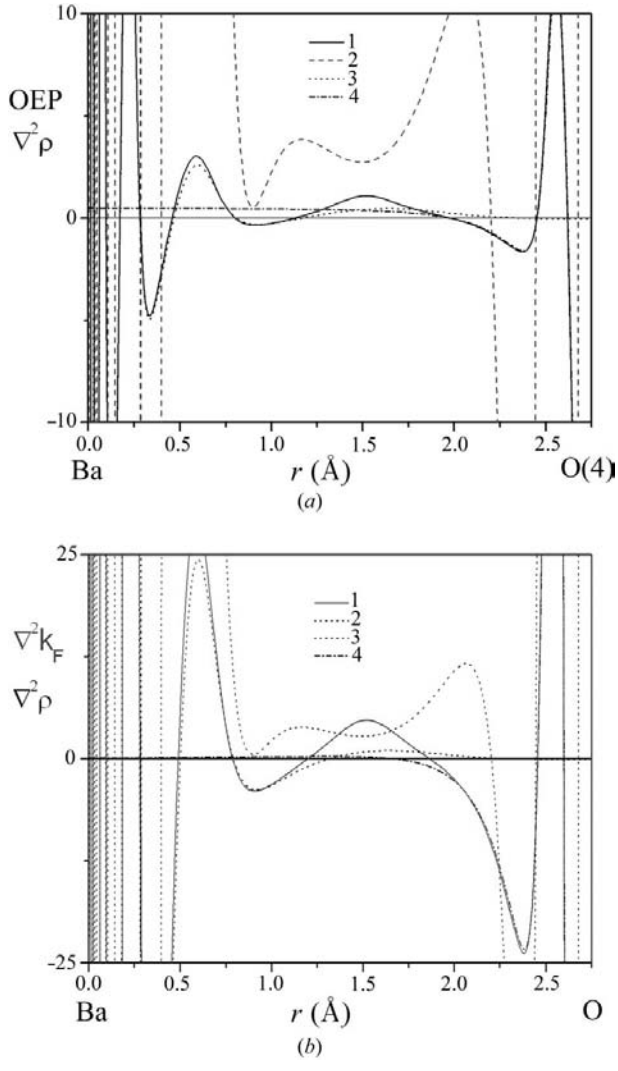

Figure 7
(*a*) Distributions of one-electron potential and (*b*) Laplacian of the local Fermi momentum along Ba—O(4) in the O—Ba—O plane of $YBa_2Cu_3O_{6.98}$: (1) one-electron potential or $\nabla^2 k_F$; (2) Laplacian of electron density; (3) and (4) contributions of Ba and O atoms to the one-electron potential or $\nabla^2 k_F$, respectively.

increases greatly the information derivable directly from X-ray diffraction data. The joint application of functions considered above to the bonding analysis looks very promising since it allows one to describe both the static charge distribution and picture the electron motion in terms of the local energy and related functions.

We thank Dr Dmitry Shorokhov for his help in the preparation of the paper. This study was supported by the Russian Ministry for High Education (grant E02-5.0-161) and the Russian Foundation for Basic Research (grant 04-03-33053). VGT thanks the Alexander von Humboldt Foundation (Germany) for a Research Award.

References

Abramov, Yu. A. (1997). *Acta Cryst.* A**53**, 264–272.
Abramov, Yu. A. & Okamura, P. F. (1997). *Acta Cryst.* A**53**, 187–198.
Aleksandrov, Yu. V., Tsirelson, V. G., Reznik, I. M. & Ozerov, R. P. (1989). *Phys. Status Solidi B*, **155**, 201–207.
Ayers, P. W., Parr, R. G. & Nagy, A. (2002). *Int. J. Quantum Chem.* **90**, 309–326.
Bader, R. F. W. (1990). *Atoms in Molecules. A Quantum Theory*. New York: Oxford University Press.
Bader, R. F. W. & Beddall, P. M. (1972). *J. Chem. Phys.* **56**, 3320–3329.
Becke, A. (1988). *Phys. Rev. A*, **38**, 3098–3100.
Bianchi, R., Gervasio, G. & Marabello, D. (2000). *Inorg. Chem.* **39**, 2360–2366.
Bone, R. G. A. & Bader, R. F. W. (1996). *J. Phys. Chem. B*, **100**, 10892–10911.
Chan, W.-T. & Hamilton, I. P. (1998). *J. Chem. Phys.* **108**, 2473–2485.
Chan, W.-T. & Hamilton, I. P. (1999). *Chem. Phys. Lett.* **301**, 53–58.
Chattaraj, P. K., Chamorro, E. & Fuentealba, P. (1999). *Chem. Phys. Lett.* **314**, 114–121.
Clinton, W. L., Frishberg, C. A., Goldberg, M. J., Massa, L. Y. & Oldfield, P. A. (1983). *Int. J. Quantum Chem. Symp.* **7**, 505–514.
Cohen, L. (1979). *J. Chem. Phys.* **70**, 788–789.
Cohen, L. (1984). *J. Chem. Phys.* **80**, 4277–4279.
Cohen, L. & Zaparovanny, Y. I. (1980). *J. Math. Phys.* **21**, 794–796.
Cramer, D. & Kraka, E. (1984). *Croatica Chem. Acta*, **57**, 1259–1281.
Dahl, J. P. & Avery, J. (1984). Editors. *Local Density Approximations in Quantum Chemistry and Solid State Physics*. New York: Plenum Press.
Dreizler, R. M. & Gross, E. K. U. (1990). *Density Functional Theory*. Berlin: Springer-Verlag.
Ellis, D. E. (1995). Editor. *Density Functional Theory of Molecules, Clusters and Solids*. Dordrecht: Kluwer Academic Publishers.
Espinosa, E., Alkorta, I., Rozas, I., Elguero, J. & Molins, E. (2001). *Chem. Phys. Lett.* **336**, 457–451.
Espinosa, E., Lecomte, C. & Molins, E. (1999). *Chem. Phys. Lett.* **300**, 745–748.
Espinosa, E. & Molins, E. (2000). *J. Chem. Phys.* **11**, 5686–5694.
Espinosa, E., Molins, E. & Lecomte, C. (1998). *Chem. Phys. Lett.* **285**, 170–173.
Galvez, O., Gomez, P. C. & Pacios, L. F. (2001). *Chem. Phys. Lett.* **337**, 263–268.
Ghosh, S. K., Berkowitz, M. & Parr, R. G. (1984). *Proc. Natl Acad. Sci. USA*, **81**, 8028–8031.
Gibbs, G. V., Boisen, M. B., Rosso, K. M., Teter, D. M. & Bukowinsli, M. S. T. (2000). *J. Phys. Chem. B*, **1004**, 10534–10542.
Gritsenko, O. B. & Zhidomirov, G. M. (1987). *Dokl. Acad. Nauk SSSR*, **293**, 1162–1165.
Hansen, N. & Coppens, P. (1978). *Acta Cryst.* A**34**, 909–921.
Hunter G. (1975). *Int. J. Quantum Chem.* **9**, 237–242.
Hunter G. (1986). *Int. J. Quantum Chem.* **29**, 197–204.
Hunter G. (1996). *Can. J. Chem.* **74**, 1008–1013.
Hill, F. C., Gibbs, G. V. & Boisen, M. B. (1997). *Phys. Chem. Miner.* **24**, 582–596.
Hohenberg, P. & Kohn, W. (1964). *Phys. Rev.* **136**, B864–B871.
Iyengar, S. S., Ernzerhof, M., Maximoff, S. N. & Scuseria, G. E. (2001). *Phys. Rev. A*, **63**, 052508.
Jayatilaka, D. (1998). *Phys. Rev. Lett.* **80**, 798–801.
Jayatilaka, D. & Grimwood, D. (2004). *Acta Cryst.* A**60**, 111–119.
Kirzhnits, D. A. (1957). *Sov. Phys. JETP*, **5**, 64–72.
Kirzhnits, D. A., Losovik, Yu. E. & Spatakovskaya, G. V. (1975). *Sov. Phys. Usp.* **18**, 649–672.
Kohn, W. (1999). *Rev. Mod. Phys.* **71**, 1253–1266.
Kohn, W. & Sham, L. J. (1965). *Phys. Rev.* **140**, A1133–A1138.
Kohout, M. (2001). *Int. J. Quantum Chem.* **83**, 324–331.
Kohout, M., Savin, A. & Press, H. (1991). *J. Chem. Phys.* **95**, 1928–1942.
Lee, C. & Zhou, Z. (1991). *Phys. Rev. A*, **44**, 1536–1539.
Levit, C. & Safarti, J. (1997). *Chem. Phys. Lett.* **281**, 157–160.
Levy, M. & Goldstein, J. A. (1987). *Phys. Rev. B*, **35**, 7887–7890.
Levy, M., Perdew, J. P. & Sahni, V. (1984). *Phys. Rev. A*, **30**, 2745–2748.
Lippmann, T., Blaha, P., Andersen, N. H., Poulsen, N. H., Wolf, T., Schneider, J. R. & Schwarz, K.-H. (2003). *Acta Cryst.* A**59**, 437–451.
Luana, V., Costales, A. & Martin Pendas, A. (1997). *Phys. Rev. B*, **55**, 4285–4297.
Lundqvist, S. & March, N. H. (1983). Editors. *Theory of Inhomogeneous Electron Gas*. New York: Plenum Press.
Macchi, P. & Coppens, P. (2001). *Acta Cryst.* A**57**, 656–662.
Martin Pendas, A., Costales, A. & Luana, V. (1997). *Phys. Rev. B*, **55**, 4575–4284.
Martin Pendas, A., Costales, A. & Luana, V. (1998). *J. Phys. Chem. B*, **102**, 6937–6948.
Nagy, A. (1998). *Phys. Rep.* **298**, 1–79.
Nagy, A. & Parr, R. G. (2000). *J. Mol. Struct. (Theochem)*, **501–502**, 101–106.
Nagy, A., Parr, R. G. & Liu, S. (1996). *Phys. Rev. A*, **53**, 3117–3121.
Reznik, I. M. (1992). *Electron Density Theory of Ground-State Properties of Crystals*. Kiev: Naukova Dumka.
Parr, R. G. & Yang, W. (1989). *Density-Functional Theory of Atoms and Molecules*. Oxford University Press.
Popelier, P. L. A. (2000). *Coord. Chem. Rev.* **197**, 169–189.
Popelier, P. L. A., Aicken, F. M. & O'Brien, S. E. (2000). *Chemical Modelling: Application and Theory*, edited by A. Hinthcliffe, Vol. 1, pp. 143–198. London: Royal Society of Chemistry.
Sagar, R. P., Ku, A. C. T., Smith, V. H. & Simas, A. M. (1988). *J. Chem. Phys.* **88**, 4367–4374.
Scherer, W. (2004). Personal communication.
Scherer, W., Sirsch, P., Shorokhov, D., Tafipolsky, M., McGrady, G. S. & Gullo, E. (2003). *Chem. Eur. J.* **9**, 6057–6070.
Schmider, H., Edgecombe, K. E., Smith, V. H. & Weyrich, W. (1992). *J. Chem. Phys.* **96**, 8411–8419.
Schwarz, K. W. E. & Mueller, B. (1990). *Chem. Phys. Lett.* **166**, 621–626.
Shi, Z. & Boyd, R. J. (1988). *J. Chem. Phys.* **88**, 4375–4377.
Spackman, M. A. (1992). *Chem. Rev.* **92**, 1769–1797.
Spackman, M. A. (1999). *Chem. Phys. Lett.* **301**, 425–429.
Springborg, M. (1977). Editor. *Density-Functional Method in Chemistry and Materials Science*. Chichester: Wiley.
Stash, A. I. (2003). Proceedings of the 28th ISTC Japan Workshop on Frontiers of X-ray Diffraction Technologies in Russia/CIS, December 2003, pp. 147–153.
Stash, A. & Tsirelson, V. (2002). *J. Appl. Cryst.* **35**, 371–373.
Stash, A., Zavodnik, V. & Tsirelson, V. (2004). In preparation.
Stevens, E. D. (1979). *Mol. Phys.* **37**, 27–45.

Suponitsky, K. Yu.,Tsirelson, V. G. & Feil, D. (1999). *Acta Cryst.* A**55**, 821–827.
Tafipolsky, M., Scherer, W., Öfele, K., Artus, G., Pedersen, B., Herrmann, W. A. & McGrady, G. S. (2002). *J. Am. Chem. Soc.* **124**, 5865–5880.
Tal, Y. & Bader, R. F. W. (1978). *Int. J. Quantum Chem. Symp.* **12**, 153–168.
Tsirelson, V. G. (1992). VI Conference on Crystal Chemistry of Inorganic Compounds, L'viv, Ukraine. Abstracts, p. 258.
Tsirelson, V. G. (2002*a*). *Acta Cryst.* B**58**, 632–639.
Tsirelson, V. (2002*b*). Conference on Electron Density: Electron Density Measurement, Calculation & Application, Wuerzburg University, Germany, p. 6.
Tsirelson, V. (2002*c*). *Acta Cryst.* A**58**, C2.
Tsirelson, V. G. (2003). 3rd Europian Charge Density Meeting and Europian Science Foundation Exploratory Workshop (ECDM-III). Sandbjerg Estate, Denmark, 2003, p. O7.
Tsirelson, V. G., Abramov, Yu. A., Zavodnik, V. E., Stash, A. I., Belokoneva, E. L., Stahn, J., Pietsch, U. & Feil, D. (1998). *Struct. Chem.* **9**, 249–254.
Tsirelson, V. G., Mestechkin, M. M. & Ozerov, R. P. (1977). *Dokl. Akad. Nauk*, **233**, 108–110.
Tsirelson, V. G. & Ozerov, R. P. (1979). *Kristallografiya*, **24**, 1156–1163.
Tsirelson, V. G. & Ozerov, R. P. (1996). *Electron Density and Bonding in Crystals*. Bristol, England/Philadelphia, USA: Institute of Physics Publishing.
Tsirelson, V. & Stash, A. (2002*a*). *Chem. Phys. Lett.* **351**, 142–148.
Tsirelson, V. & Stash, A. (2002*b*). *Acta Cryst.* B**58**, 780–785.
Tsirelson, V. G., Zhou, P. F., Tang, T.-H. & Bader, R. F. W. (1995). *Acta Cryst.* A**51**, 143–153.
Zhao, Q. & Parr, R. G. (1993). *J. Chem. Phys.* **98**, 543–548.
Zhurova, E. A. & Tsirelson, V. G. (2002). *Acta Cryst.* B**58**, 567–575.